This chapter focuses mostly on the usage of Amberlite IRA-400(Cl^-) resin as an adsorbent for the elimination of AY 49 and RO 12. It is characterized of after and before sorption using FTIR, XRD, SEM-EDX and UV-vis. These dyes adsorption batch process onto adsorbent is discussed in this chapter.

4.1. Introduction

Among the various known forms of pollution, Water pollution is one of the largest and most significant problems of our time. Nowadays, water contamination associated with dyes is distinguished as among the most critical global challenges and has attracted increasing concern all over the world [1]. In the textile dyeing processes, a large volume of azo dye-contaminated effluent is discharged, and it was estimated that 7-20% of acid dyes and 20-50% of reactive dyes were lost in the effluents [2]. Even at very low quantities, the presence of these dyes in water is highly apparent and disregarded. There are demonstrable facts that the dye effluents of textile industry are posing a serious harm to aquatic living organisms [3]. Consequently, the elimination and prior treatment of this coloured pollutant are essential and challenging. Moreover, most textile dyes are large molecules (formed by a combination of aromatic rings connected by different chromophores) that often are resistant to various methods. As consequently, multiple methods have been developed to remove dyes [4–7]. Among the multitude of conventional methods, adsorption is belonging to the most efficient, flexibility and insensitivity to toxic substance and well-designed sorption process of eliminating pollutants from wastewater, particularly when the adsorbent is universally accessible and affordable. Extensive research on dye removal has been reported in the literature, owing to the variety of adsorbents and their ease of implementation [8,9]. Studies employing activated carbon, activated carbon generated from wood scraps, silica gel, fly ash, carbon nanotubes, metal-organic frameworks, nanoparticles, and other materials [10–13].

Among all materials, ion exchange resins in recent times are regarded as the most promising adsorbent substances due to their chemical stability, capacity to regulate physical stability and surface chemistry for targeted temperatures while dealing with aqueous solutions [14,15]. Among various synthetic resins, favorable sorption outcomes applying anion exchange resin with different basicity and matrix configurations imply that they might be effective sorbents for the removal of azo dyes [16]. It is freely accessible and affordable as well. The features of the adsorbents and their structure play a major role in the adsorption of dyes [17].

As acid and reactive dyes have electronegative sulfonic groups in their molecular structure, they are easily removed by anion-exchange resin through electrostatic attraction [18]. The source material offers helpful details about the applicability of anion exchange resin for the elimination of dyes from aqueous solutions [19]. Researchers have been working on the eradicate of several dyes (Acid Orange 7, Reactive Black 5 [20], Acid Orange 7 and Acid Orange 10 [21], Acid Red 18 and Reactive Blue 21 [22], Acid Blue 29 [23], Reactive Remazol Black B [24], Acid Green 16 [25] using different kinds of adsorbents Dowex PSR-2 and Dowex PSR-3, Amberlite IRA-900 and Amberlite IRA-910, Amberlite IRA 478, Purolite A-520E, Amberlyst A 23 and Lewatit S 6368.

Among these resins, a strongly base anion exchange resin; Amberlite IRA-400(Cl^-) resin was used an adsorbent in this investigation. These polymeric resins are cross-linked, highly macroporous, insoluble and maintains the porosity of particles. Acid Yellow 49 (AY 49) and Reactive Orange 12 (RO 12) were selected as model acid and reactive dyes. AY 49 is a brilliant yellow azo dye extensively employed in the dyeing industries. RO 12 is yellow orange azo may be utilized for cotton, hemp, silk, viscose, nylon fabric dyeing, knot dyeing, etc.

The goal of this study is to investigate the removal efficacy of AY 49 and RO 12 dye onto Amberlite IRA-400(Cl^-) resin in a batch method under multiple operating conditions (pH, dose of adsorbent, initial concentration of dye, contact time and temperature) and it's characterized by EDX, SEM and FTIR. The relevance of useful isotherms (Langmuir and Freundlich) and models of kinetics [pseudo-first-order, pseudo-second-order and intra-particle-diffusion] were utilized for the modelling of experimental data. The adsorption rate constants were acquired at different temperatures to estimate the dye adsorption's thermodynamic parameters.

4.2. Experimental section

4.2.1. Materials and characterization techniques

"Chapter 2" provides a thorough interpretation of all the chemical ingredients and instruments used in this work (Section 2.1 & 2.3).

4.2.2. Adsorbent and adsorbate preparation and calibration

The economically viable and commercially accessible adsorbent as strongly base anion exchange resin, Amberlite IRA-400(Cl^-). To get rid of any impurities, deionized water was used to wash the resin. The washed resin was left overnight for air-drying at 30^0C for 24 h. The resin was procured and stored in a desiccator at room temperature until use. Before being used, the resin was acquired and kept at room temperature in a desiccator.

Acid yellow 49 (AY 49) and Reactive orange 12 (RO 12) were used as adsorbate. A stock solution (1000 mg/L) of AY 49 and RO 12 dyes were made using deionized water. The maximal absorbance at λ_{max} = 408 nm for AY 49 and λ_{max} = 417 nm for RO 12 before and after treatment were using UV-vis spectrophotometer. After that, the curves of calibration for these two dyes had been established, from which the slope of the derived absorbance-concentration lines might be used to estimate precise concentrations. Employing a UV-Vis spectrophotometer, the calibration curves of AY 49 and RO 12 dyes investigated in the current work are depicted in **Figure 4.1**.

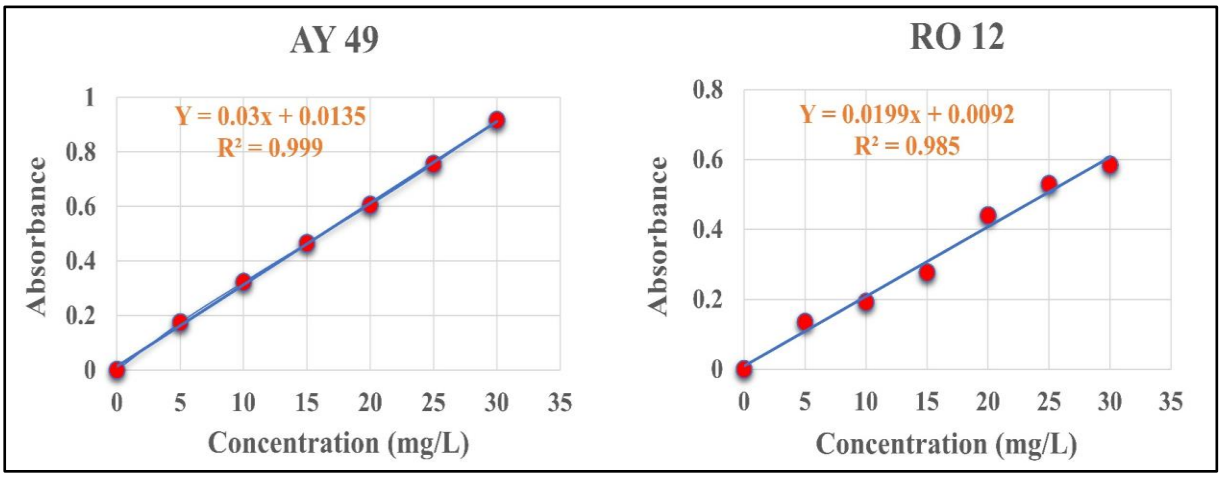

Figure 4.1. The Calibration Curve for Acid Yellow dye (AY 49) and Reactive Orange 12 (RO 12).

4.2.3. Adsorption Study

The consequence of several aspects, such as pH throughout the interval of 2-11, adsorbent dosage (10-200 mg/L), initial concentration of dye (10-300 mg/L), duration of contact (5-240 min) and temperature of 300-333 K on the adsorptive elimination of AY 49 and RO 12 were investigated by batch experiments. Adsorption experiments have been conducted

in a series of 100 mL conical flask containing 20 mL solution and adsorbent using a rotary incubator shaker at a speed of 120 rpm. After adsorption, every flask's contents were carefully decanted into a dry, clean flask. Final concentrations of AY 49 and RO 12 dye in solution analyzed by spectrophotometrically at a certain wavelength after separation of adsorbent. Triplicate repetitions of each experiment were carried out. The adsorption process's kinetics, thermodynamic, and isothermal characteristics were assessed and computed by fitting the acquired experimental data at various times, temperatures, and concentrations using various models. The required pH was raised with 0.1 M HCl or 0.1 M NaOH solution. The percentage of removal [R (%)] for AY 49 and RO 12 were computed with the subsequent equation.

$$\textbf{Removal efficiency } (R\%) = \frac{(C_o - C_e)}{C_0} \times 100 \quad (1)$$

The amount of AY 49 and RO 12 dye adsorbed, at equilibrium (q_e), with Equations (2), respectively:

$$q_e = \frac{(C_0 - C_e)\, V}{W} \quad (2)$$

Where C_o, C_e represent the concentration of AY 49 and RO 12 dye initially and at time t, and at an equilibrium (mg/L), respectively. q_e denotes adsorption at t equilibrium (mg/g). W is the weight of the adsorbent (g); and V is the solution's volume (L).

4.2.3.1. Adsorption isotherm

The studies of equilibrium are crucial in optimizing the design parameters for any adsorption system and provide sufficient information on the physicochemical data in evaluating the process of adsorption as a unit operation. Studies using isotherms were conducted by varying the initial concentration of the aqueous dye mixture solution at room temperature. Finding the best feasible correlation between the experimental data and the isotherm model is crucial for learning about the features of the mechanism. The equilibrium mechanisms in these investigations have been illustrated by the Freundlich and Langmuir models.

A. **Langmuir isotherm model:** When an adsorbate is adsorbed in a solution, the Langmuir isotherm describes the adsorption as monolayer adsorption with a finite number of unique sites and uniform energies. The most prevalent and fundamental adsorption equation is the Langmuir adsorption isotherm [26,27]. The following is the Langmuir isotherm equation in linear form (Equation 3),

$$\frac{1}{q_e} = \left[\frac{1}{K_L(q_{max})}\right]\frac{1}{C_e} + \frac{1}{q_{max}} \quad (3)$$

where K_L refers to the equilibrium constant of Langmuir adsorption and the maximal adsorption capacity is denoted by q_{max}, C_e represents equilibrium dye concentration (mg/L), In the equilibrium state, q_e represent the quantity of AY 49 and RO 12 adsorbed per unit mass of the adsorbent (mg/g). Plotting $1/q_e$ vs $1/C_e$, which is anticipated to produce a linear pattern, is used to justify the experimentally acquired data for the adsorption of AY 49 and RO 12 dye. The Langmuir fitting model may be used to get the values of K_L and q_{max}.

Equation (4) defines the separation factor R_L, which is a crucial component of the Langmuir equation.

$$R_L = \frac{1}{1 + C_0 K_L} \quad (4)$$

where C_0 is the greatest initial dye concentration (mg/L), and Langmuir constant (L/mg) is denoted by K_L. Additionally, the geometry of the isotherm is determined by the value of the dimensionless R_L coefficient: favourability of adsorption: $0 < R_L < 1$, favourable; $R_L > 1$, unfavourable; $R_L = 1$, linear; and $R_L = 0$, irreversible [28].

B. Freundlich isotherm model: A well-characterized experimental equation for adsorption on the energetically heterogeneous surfaces of adsorbents is the Freundlich isotherm. The term is employed to characterize reversible adsorption and is not limited to the creation of a single layer [29]. Equation (5) provides a description of the Freundlich model.

$$\log q_e = \log k_f + \frac{1}{n \log C_e} \quad (5)$$

where K_F indicate the capacity of Freundlich adsorption (mg/g), n denote Freundlich constant associated with the heterogeneity of the surface, C_e represents the dye concentration at equilibrium (mg/L) and q_e is the quantity of AY 49 and RO 12 adsorbed in the equilibrium state per mass unit of the adsorbent (mg/g).

The plots of log q_e vs. log C_e have been employed to estimate the values of the Freundlich parameters. An integer of $1/n < 1$ denotes a strong adsorption bond resulting from strong intermolecular attractions in the adsorbent layers, whereas a value of $1/n > 1$ implies a weak connection between the adsorbate and adsorbent molecules [30].

4.2.3.2. Kinetics of sorption

The adsorption kinetics of AY 49 and RO 12 dye with Amberlite IRA-400(Cl^-) resin have been examined via altering the adsorption equilibrium's contact time. The sorption of data fitting for AY49 and RO12 on the Amberlite IRA-400(Cl^-) resin have been examined by three prominent models of kinetics, namely, the pseudo-first-order model, pseudo-second-order model and Weber-Morris intraparticle diffusion model was as described earlier in Chapter 3 (Sec. 3.2.4, 3.2.4.1, 3.2.4.2, 3.2.4.3).

4.2.3.3. Study of thermodynamics

Adsorption thermodynamics was the main focus of adsorption investigations in order to determine the adsorbent's affinity for the adsorbate. The process's stability and spontaneity are reflected in the thermodynamic attributes. By utilizing various parameters of thermodynamics for the present system, including standard change in Gibbs free energy (ΔG^0, kJ/mol), standard enthalpy change (ΔH^0, kJ/mol), and standard entropy change (ΔS^0, J/mol K) were computed using the subsequent equations, as previously reported [31].

$$\Delta G^o = -RT \ln K_L \quad (6)$$

$$\ln K_L = \frac{\Delta S^o}{R} + \frac{\Delta H^o}{RT} \quad (7)$$

where the equilibrium dye concentration (C_e) in mg/L and equilibrium dye adsorption (q_e) in mg/L can be used to derive K_L, the thermodynamic equilibrium constant. R is the universal constant of gas (8.314 J/mol.K), T is the precise temperature (K). A van't Hoff plot of ln K_L vs. 1/T was used to find ΔS^o and ΔH^o from the intercept and the slope, respectively,

4.3. Results and discussion

4.3.1. Characterization of Amberlite IRA-400(Cl^-) resin

4.3.1.1. FESEM and EDS Analysis

The surface morphological examination of the adsorbent, both before and after adsorption, was examined using SEM analysis in order to validate the adsorption mechanism. It is evident from the characteristic changes in phase presented in **Figure 4.2 (a-c)** that dyes adsorb onto the surface of the adsorbent, which is (Amberlite IRA-400(Cl^-) resin). Before sorption, the resin phase's surface morphology presented a rigid structure; however, AY 49 and

RO 12's adsorption onto the Amberlite IRA-400(Cl^-) resin resulted in a substantial alteration in the resin phase's morphology. After adsorption with AY 49 and RO 12, the dye molecules bond to the Amberlite IRA-400(Cl^-) resin sites, causing the adsorbent surface to take on a porous, uniform pattern. EDX spectra and element table of Amberlite IRA-400(Cl^-) resin is illustrated in **Figure 4.3** to identify the chemical composition.

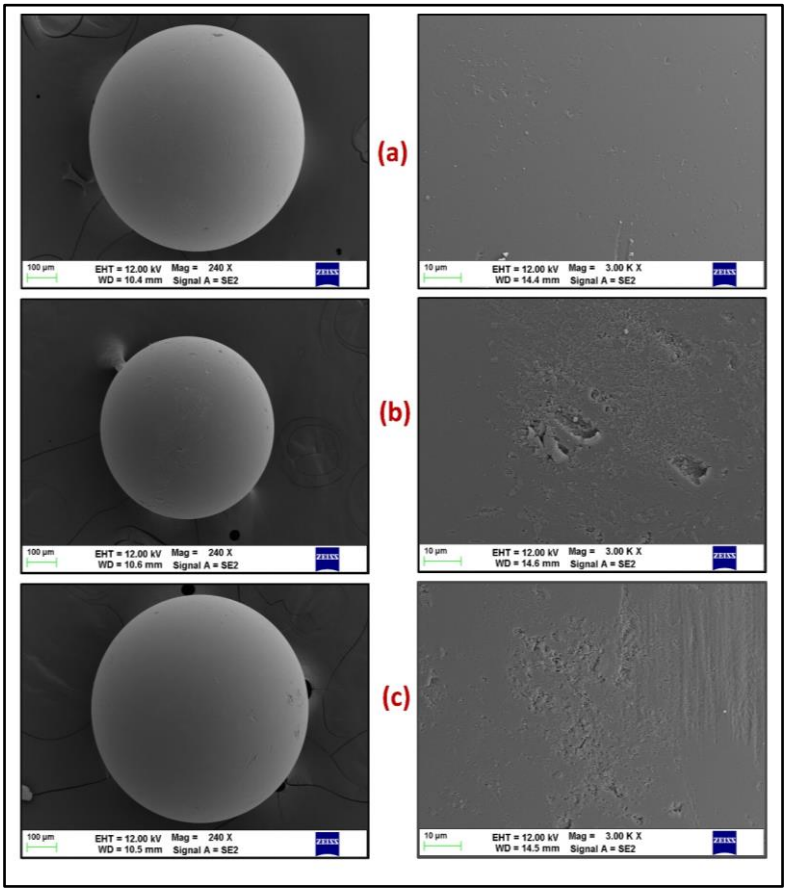

Figure 4.2. FESEM image of (a) Amberlite IRA-400(Cl^-) resin (b) AY 49@Amberlite IRA-400(Cl^-) resin and (c) RO 12@Amberlite IRA- 400(Cl^-) resin.

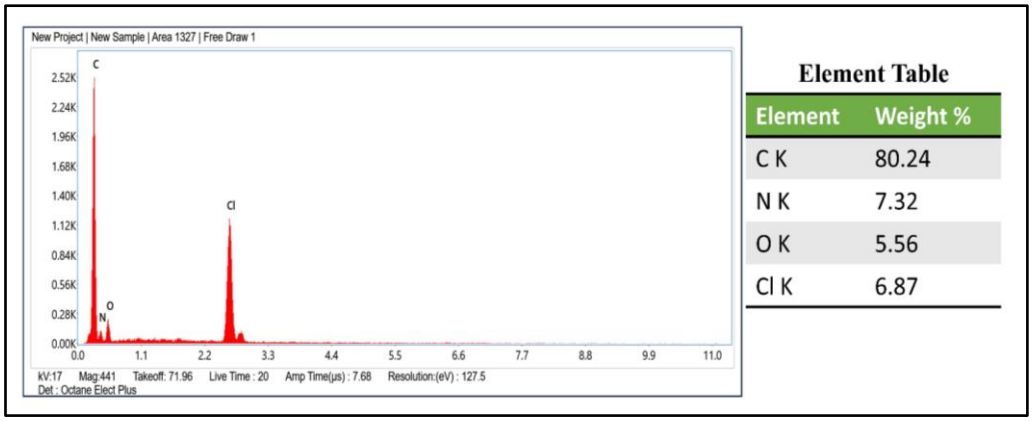

Figure 4.3. EDS Spectra of before sorption of Amberlite IRA-400(Cl^-) resin.

4.3.1.2. XRD Analysis

The adsorbent's XRD patterns appeared in the 20^0-80^0 2θ range both before and after sorption **(Figure 4.4)**. No sharp peaks were observed in the diffraction profiles, indicating the dominance of an amorphous structure. The absence of distinct peaks or the presence of broadened peaks indicates the formation of an amorphous phase.

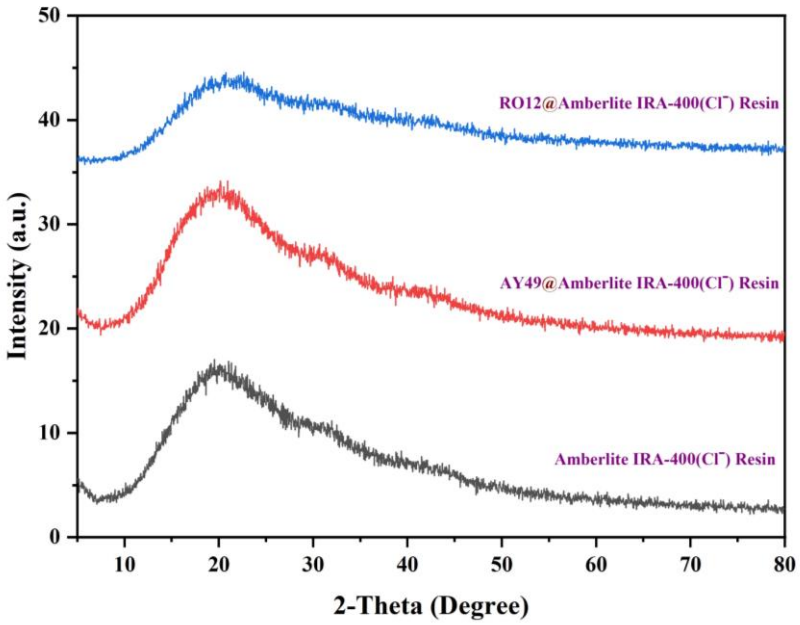

Figure 4.4. XRD curve of Amberlite IRA-400(Cl^-) resin, AY 49@ Amberlite IRA-400(Cl^-) resin and RO 12@ Amberlite IRA-400(Cl^-) resin.

4.3.1.3. FTIR Analysis

Figure 4.5 illustrates the collected FT-IR spectra before and after the sorption of Amberlite resin IRA-400(Cl^-) resin. This exhibited a range of absorption bands that complemented the correct functional groups. Due to the presence of water in the anion exchanger phase, the wide band characteristic for -OH vibrations of stretching emerged before to the resin exhibiting at 3628 cm^{-1}. The stretching vibrations of the C-H and -CH_2 groups in the aromatic rings of the matrix are responsible for the peak that was detected at 3028 cm^{-1} and 2930 cm^{-1}. The presence of amines was confirmed by the sharp peaks observed at 1220 cm^{-1} (C-N stretching vibration) and at 976 cm^{-1} (C-N) [32]. The peak was discovered at approximately 1747 cm^{-1}, which corresponds to the stretching of C=O groups. Moreover, the peaks at 1487 cm^{-1} correlated to the existence of quaternary ammonium groups of polystyrene resin. The intensity of specific bands changed after the sorption of AY 49 and RO 12.

The spectra of after sorption revealed the appearance of symmetric and asymmetric vibrations of sulfonic $-SO_3^-$ groups at1085 and 1146 cm^{-1}, respectively. Additionally, an asymmetric vibration of the –S=O group was discovered at 1013 cm^{-1}. It appears that these groups engage in the process of dye binding [33]. It might suggest that the development of an ionic couple between the sulfonic groups of the dye and the functional groups of the resin is what causes the dye's retention mechanism. By comparing resin's FTIR spectra and the dye-resin complex before and after sorption, changes in peak intensities or shifts can indicate the development of new bonds or interactions between molecules of dye and the resin functional groups.

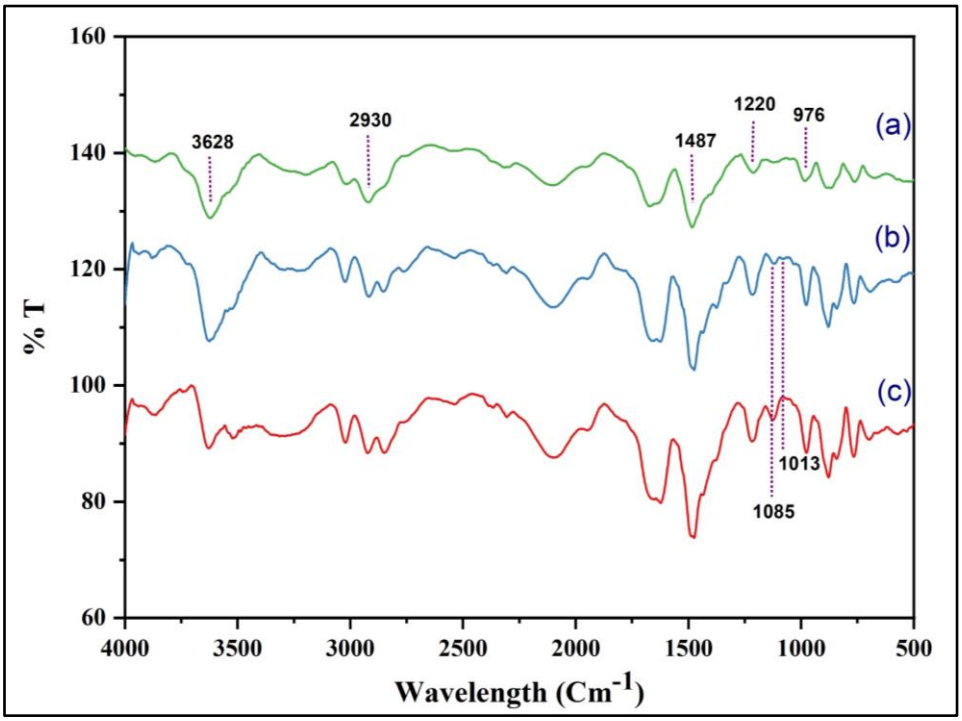

Figure 4.5. FTIR Spectra of (a) Amberlite IRA-400(Cl^-) resin (b) AY 49@Amberlite IRA-400(Cl^-) resin and (c) RO 12@Amberlite IRA- 400(Cl^-) resin.

4.3.2. Evaluation of various parameters of adsorption

4.3.2.1. Influence of pH on sorption of AY 49 and RO 12

To experimentally quantify how pH influences AY 49 and RO 12 adsorption on Amberlite IRA-400(Cl^-) resin as an anion exchange resin, batch studies were evaluated in the pH ranges of 2 to 12 at room temperature for 60 min with a 100 mg dosage and (50 mg/L) dye concentration of initial dye. An extremely crucial factor governing the sorption processes is the solution's pH. The solution's acidity or basicity has a significant effect on the ion exchange

process. The dye solution's pH value affects its ionic form, or the extent to which functional groups dissociate, and consequently the type of interaction that occurs between the adsorbent and adsorbate. **Figure 4.6** illustrates the dependences of dye uptake with initially pH. As can be shown, during the whole pH range of 2 to 11, the adsorption of AY 49 and RO 12 on the adsorbent remained essentially unaltered. The highest removal for both dye dyes was accomplished at a natural pH of 4.15 for AY 49 and 4.07 for RO 12. Thus, this pH was chosen as working condition in next experiments. The adsorption mechanism was substantially facilitated by the formation of ion pairs as an outcome of the electrostatic attraction between the dyes and the quaternary ammonium groups of strongly basic anion exchangers across the whole pH range [34,35]. A similar phenomenon was reported in [36].

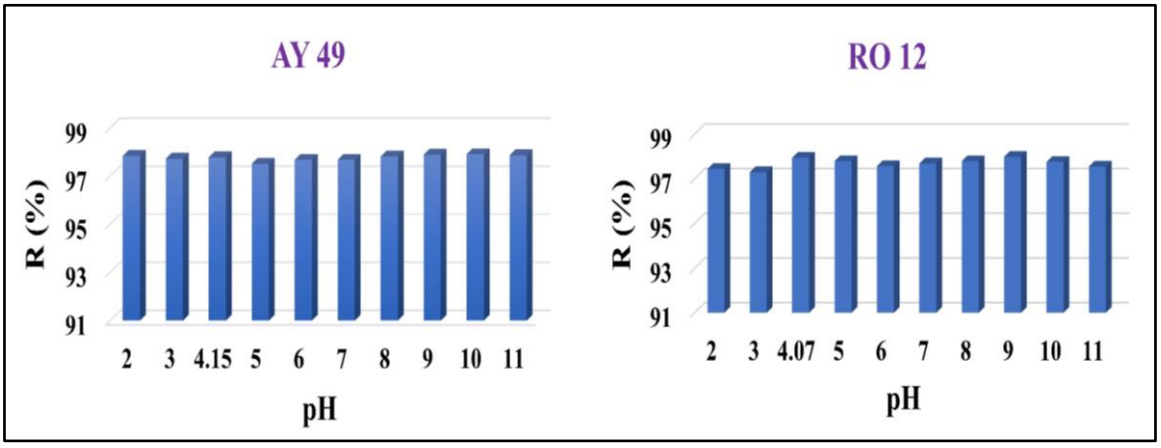

Figure 4.6. Effect of pH for after sorption of AY 49 and RO 12 onto adsorbent.

4.3.2.2. Influence of dose of adsorbent on sorption of AY 49 and RO 12

The dose limitations of the adsorbent indicate its capacity and its capability to remove each in a quantitative manner for a specific beginning concentration [37]. A batch test was performed to ascertain the ideal resin amount needed to remove AY 49 and RO 12. Therefore, different resin loads in a solution containing 50 mg/L of AY 49 and RO 12, at 30 ^{0}C and optimised pH after 60 minutes of contact period were used as initial conditions. There was a change in the resin dosage from 10 to 200 mg. **Figure 4.7** shows that the maximal adsorption of AY 49 and RO 12 were obtained at 80 mg/L resin dose, reaching 98 % of AY 49 and 96.3 % of RO 12 removal. Adsorption increases quickly as the mass of the adsorbent increases, resulting in increased surface area and more adsorption sites being available. Increased adsorbent dosage causes fewer dye molecules to occupy the unoccupied space, which increases dye molecule migrating and diffusion to the adsorbent surface. After the maximum removal

(98%, 96.8%), the percentage of dye removed does not change significantly when the adsorbent dosage is raised. This removal was clarified by the attractive interplay between the groups of ammonium quaternaries of Amberlite IRA-400(Cl^-) resin and the sulfonate groups of AY 49 and RO 12. Consequently, the optimal resin dosage for the quantitative removal of AY 49 and RO 12 was determined to be 80 mg of adsorbent and were kept the same for all the studies. Similar outcomes are documented in [38].

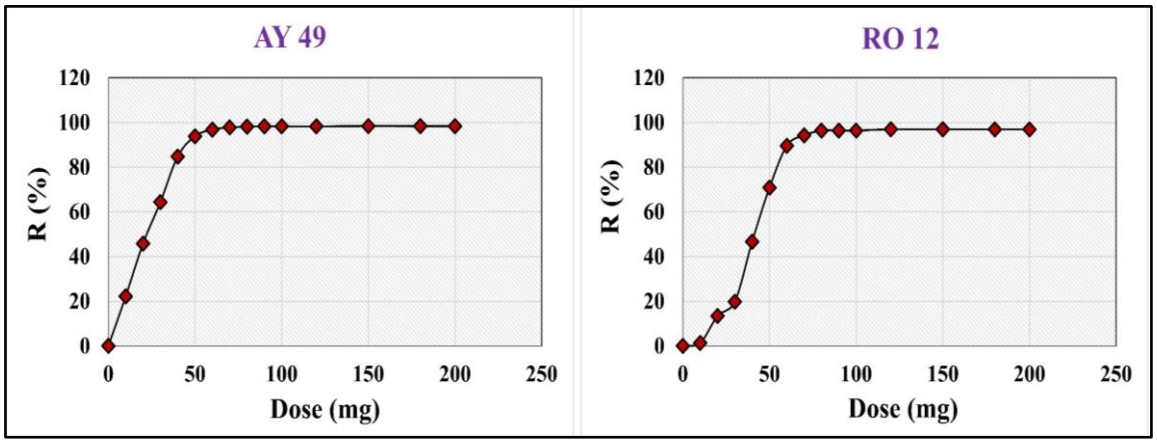

Figure 4.7. Effect of dose for after sorption of AY 49 and RO 12.

4.3.2.3. Influence of initiating concentration on sorption of AY 49 and RO 12

The impact of AY 49 and RO 12 concentrations ranging from 10 to 300 mg/L on the adsorption of the materials by Amberlite IRA-400 (Cl^-) resin was examined, and **Figure 4.8** shows the percentage of AY 49 and RO 12 removal at various initial concentrations. The investigation was done at optimized adsorbent doses (80 mg/L) in the test solution, at room temperature and optimised pH for 60 min. It appears that as the initial dye concentration increased, the percentage of AY 49 and RO 12 dye removal reduced, indicating that the initial concentration of the dyes was a determining factor in the adsorption of the dyes from their aqueous solutions. Further experiments were conducted using the 50 mg/L concentration, as it was observed to have the best adsorption outcomes. A saturation of the adsorbent's accessible active sites may be the cause of this decrease in removal efficiency. A higher solute to adsorbent empty sites ratio leads to more elimination of colour at lower dye concentrations [36, 39].

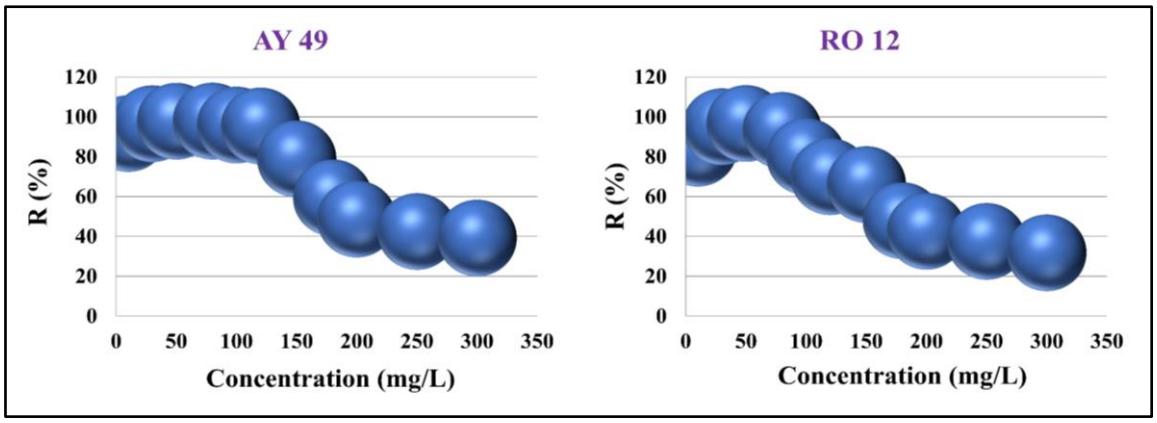

Figure 4.8. Effect of concentration for after sorption of AY 49 and RO 12.

4.3.2.4. Influence of contact time on AY 49 and RO 12 sorption

One of the crucial factors in the design of an affordable wastewater treatment system is equilibrium time. The relation between adsorption of AY 49 and RO 12 onto Amberlite IRA-400 (Cl^-) resin and duration of contact (5-240 min) were examined to establish the rate of dye removal. **Figure. 4.9** shows the percentage removal of AY 49 and RO 12 at 50 mg/L initial dye concentrations, optimized dose (80 mg), natural pH and room temperature. **Figure. 4.11 and Figure. 4.12** shows that UV adsorption spectra of AY 49 and RO 12.

According to the experimental results, the percentage of removal of AY 49 and RO 12 dye increased with increase contact time. In the first 40 min, the percentage removal of AY 49 (97%) and RO 12 (92.3%) dye was very high and thereafter, it proceeds at a slower rate and reached equilibrium. The fast treatment of these dyes in the first 40 min may be due to the availability of vacant sites at the Amberlite IRA-400(Cl^-) resin surface. This reaction was observed due to the binding of AY 49 and RO 12 dye to the Amberlite IRA-400 (Cl^-) resin active sites and functional groups, which gradually reached to saturation [40]. Comparable outcomes have been found in [41].

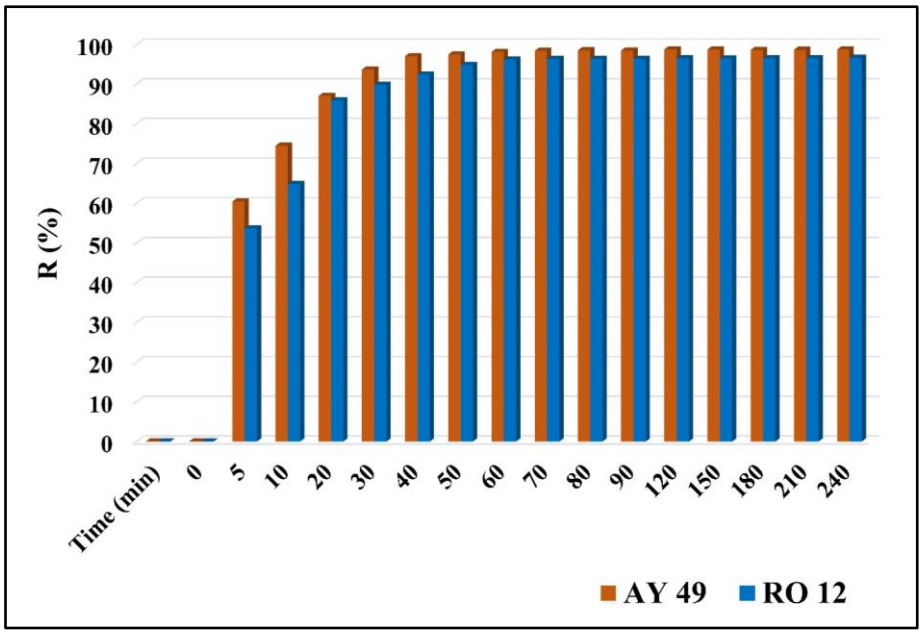

Figure 4.9. Effect of time for after sorption of AY 49 and RO 12.

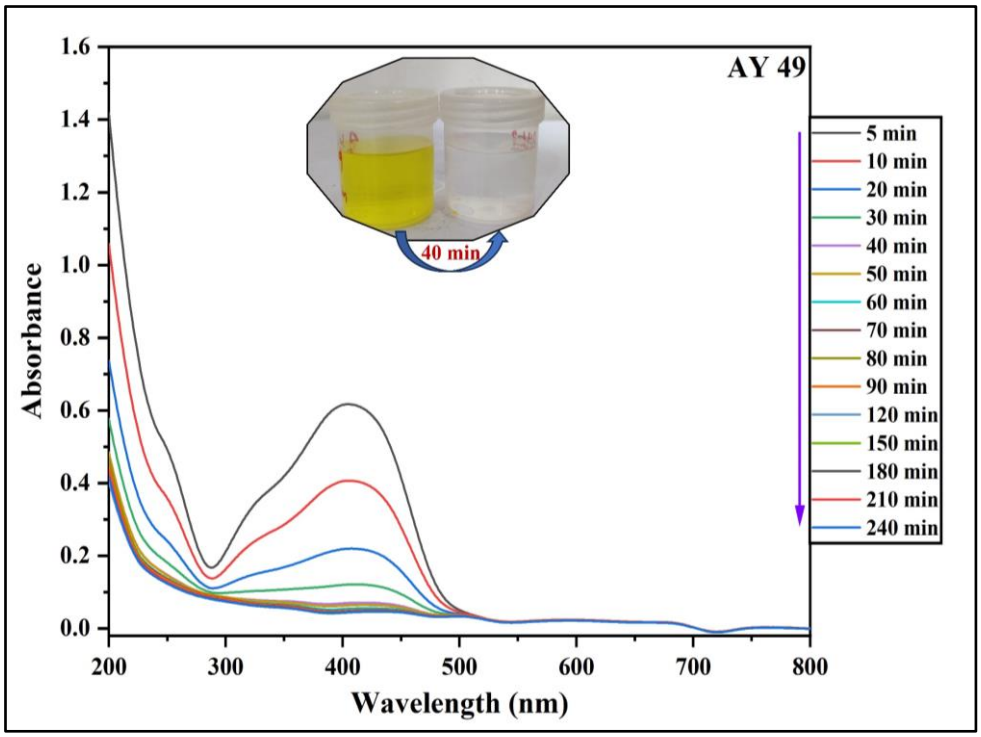

Figure 4.10. UV adsorption spectra for after sorption of AY 49.

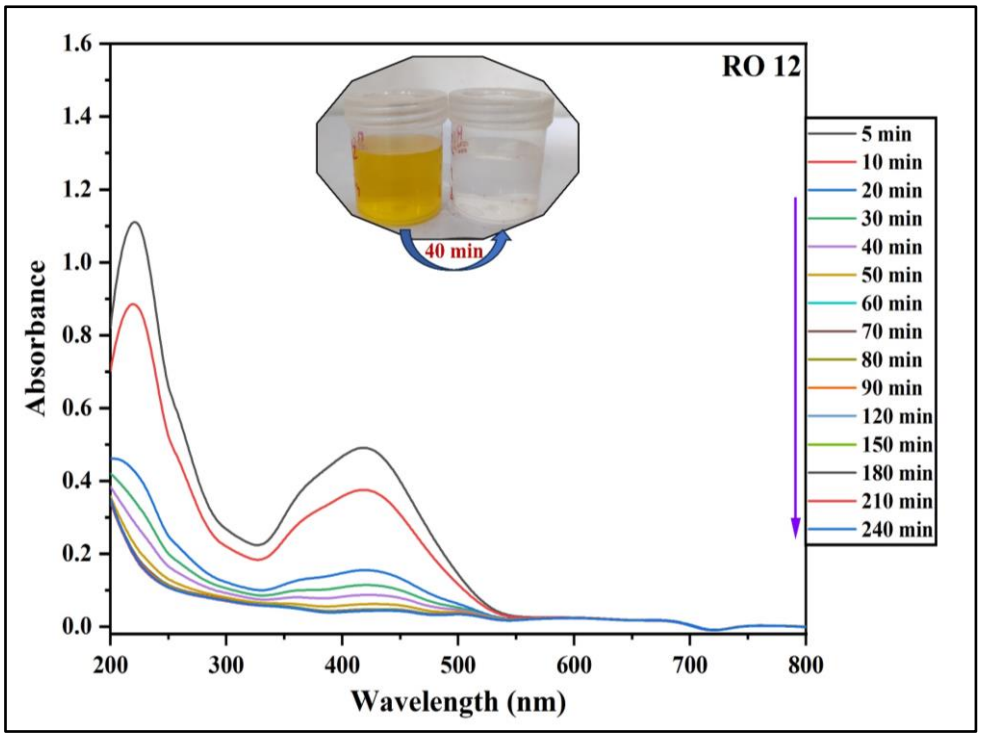

Figure 4.11. UV adsorption spectra for after sorption of RO 12.

4.3.2.5. Influence of temperature on sorption of AY 49 and RO 12

A crucial factor in the real-world utilization of anion exchangers is temperature [47]. The evaluations have taken place by dynamic method at various temperatures ranging from 30 to 60 °C with a quantity of adsorbent of 80 mg, 50 mg/L initial dye concentrations, natural pH and contact period of 40 min, respectively. The data obtained in this study **(Figure 4.12)** shows that the uptake of AY 49 and RO 12 on Amberlite IRA-400(Cl^-) resin as a function of temperature under static conditions, % R of AY 49 and RO 12 slightly increases with the rising temperature. The enhancement in adsorption with temperature might be illustrated by the increased number of active centers from the sorbent and also by the increase in the porosity and pore volume. The reality that dye sorption is in favour of temperature indicates that the mobility of the molecules containing the dye increases with the temperature rise. Thus, the additional trials were conducted at 30 °C since there is a very slight increase in sorption between 30 and 40°C and no variations are observed when conducting at 40°C or 50°C. Similar occurrences have been recorded in [42,43].

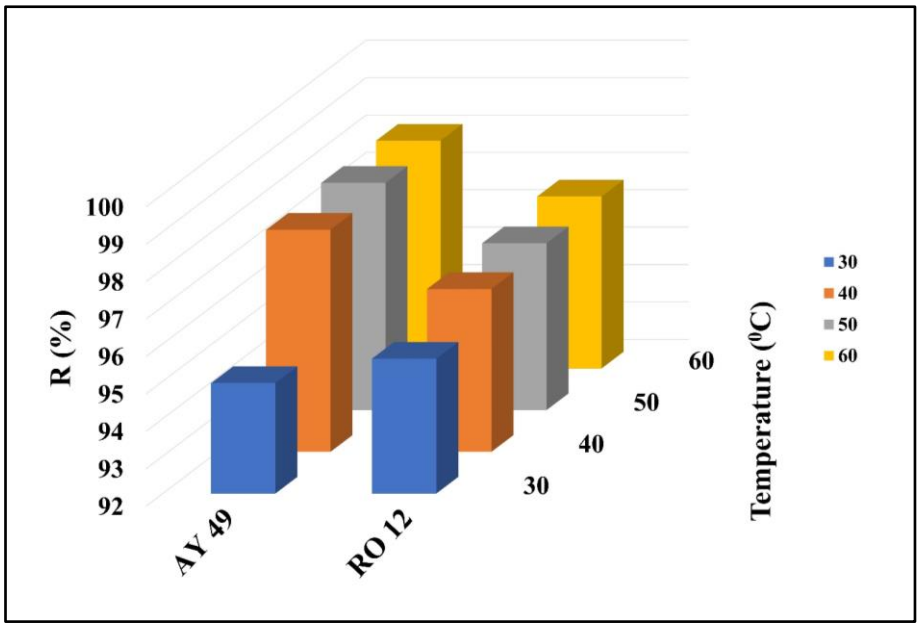

Figure 4.12. Effect of temperature (30-60^{0}C) for after sorption of AY 49 and RO 12.

4.3.2.6. Langmuir and Freundlich Isotherm model

To ascertain the sorption effectiveness of AY 49 and RO 12 onto Amberlite IRA-400(Cl^-) resin at equilibrium state, the specified parameters were computed and the $1/q_e$ vs. $1/C_e$ and $\log(q_e)$ vs. $\log(C_e)$ plots were drawn **(Table 4.1)**. **Figure. 4.13 and 4.14** illustrate how the adsorption models discussed above were modified in light of the experimental findings. A determination coefficient of R^2 was used to assess the applicability of the isotherm equations. For the AY 49, RO 12 sorption on resin, the R^2 values obtained from the $1/q_e$ vs. $1/C_e$ plots were 0.506 and 0.507, respectively. For the sorption of AY 49 and RO 12 on resin, the corresponding estimation coefficients of the Freundlich sorption isotherm were 0.783 and 0.763. Still, the comparison of the R^2 values shows that the Freundlich isotherm model was more suited to the experimental data of RO 12 and AY 49 adsorption onto Amberlite IRA-400(Cl^-) resin. It was discovered that the Amberlite IRA-400(Cl^-) resin has monolayer sorption capacities of 2000 mg/g for AY 49 and 175.43 mg/g for RO 12. It may be consistent with the RO 12 and AY 49 dyes' propensity to aggregate, particularly at elevated concentrations, and the probability of dye absorption through a variety of interactions. However, the Langmuir and Freundlich isotherm models' respective values of R_L and 1/n were found to be between 0 and 1, implying that the adsorption process was preferred. The mechanism of dye sorption is mediated by the π-π type interactions between the aromatic ring in the dye structure and the resin matrix, as well as the creation of ionic pairs between the positive functional groups of the resin and the sulfonic groups of the negative charge of the dye.

The results indicate that AY 49 dye has the maximum affinity for the Amberlite IRA-400(Cl^-) resin. The following is an explanation of resin's dye affinity based on the investigations that were carried out: AY49 > RO12. The fact that AY 49 has the highest value indicates that it has a strong binding with the Amberlite IRA-400(Cl^-) resin, a polystyrene anion exchanger. Due to its smaller size when compared to RO 12 dye, the resin exhibits the highest affinity for AY 49. A "sieve effect" occurs when the species are excluded from the resin phase due to an excessively large dye anion. Similar observations were described in [44,45]. On the basis of the existing literature, the q_{max} value of Amberlite IRA-400(Cl^-) resin is much better than other adsorbents, like Amberlite IRA-958 for Acid Orange 7 (1370 mg/g) [46], Amberlite IRA-900 and Amberlite IRA-910 for Tratrazine (57.6 mg/g, 44.63 mg/g) [47], Polystyrene anion-exchange resin SAER and Polyacrylic anion-exchange resin AAER for Acid Orange 10 (670 mg/g, 855 mg/g) [48], Purolite A-520E for Acid Blue 29 (321.5 mg/g) [23].

Table 4.1. Linear Langmuir and Freundlich Isotherm Model parameters for the Adsorption process at 303 K.

Dyes	Langmuir constants				Freundlich constants		
	R^2	K_L ($L.mg^{-1}$)	Q_{max} ($mg.g^{-1}$)	R_L	R^2	K_f ($mg.g^{-1}$)	n
AY 49	0.506	0.0038	2000	0.839	0.783	12.67	1.67
RO 12	0.507	0.019	175.43	0.507	0.763	0.019	1.32

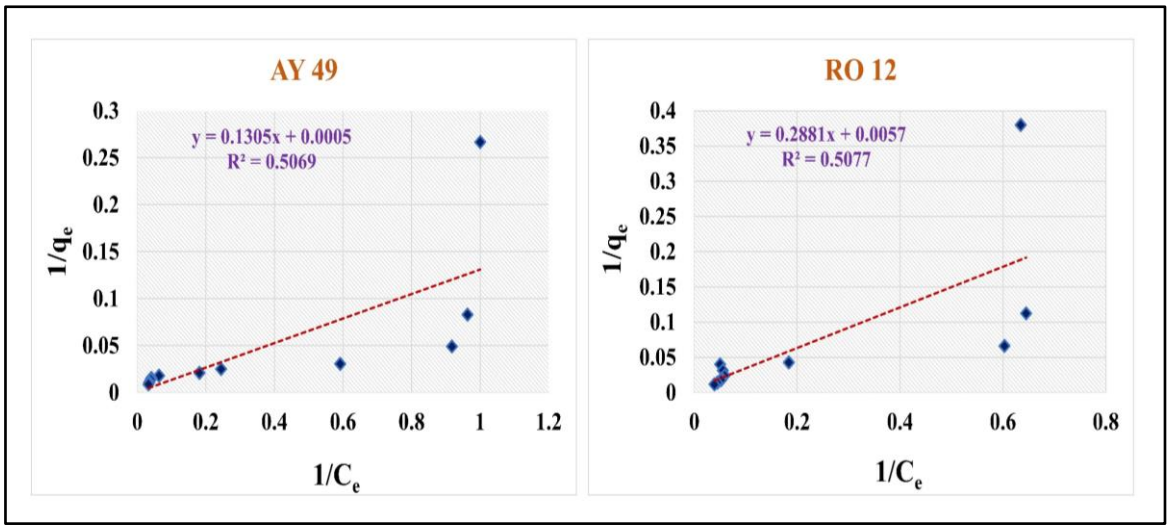

Figure 4.13. Langmuir Isotherm for sorption of AY 49 and RO 12.

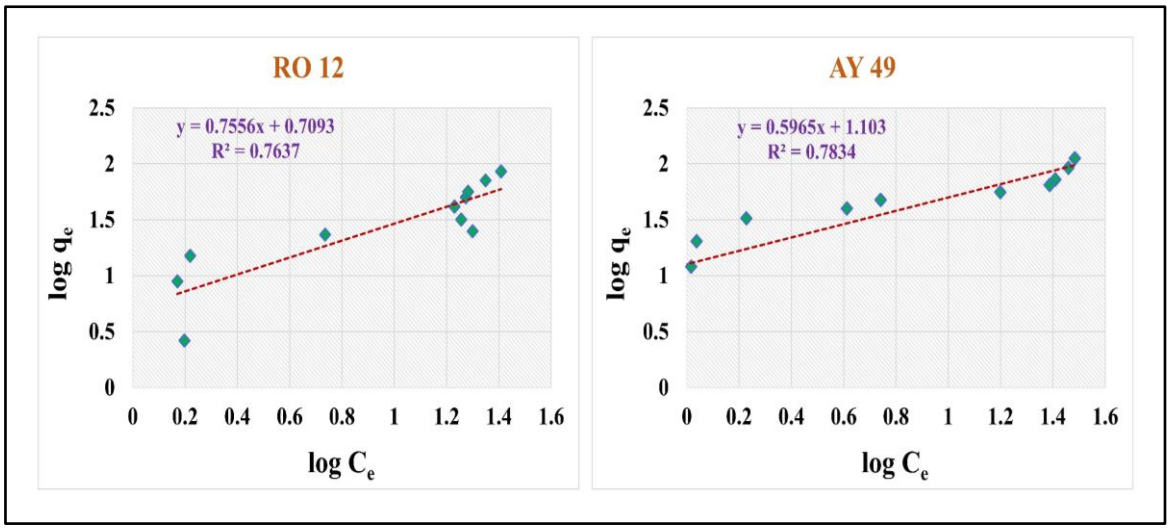

Figure 4.14. Freundlich Isotherm for sorption of AY 49 and RO 12.

4.3.2.7. Kinetics of sorption

In light of the determined kinetic parameters, listed in **Table 4.2**, it is possible to determine which model is most compatible. **Figure 4.15 and 4.16** illustrate distinctive adsorption behavior at various points in time for the pseudo-first-order kinetic model, pseudo-second-order kinetic model and Weber-Morris intraparticle diffusion model that were fitted with the experimental results. Based on this outcome, it was discovered that the pseudo-second-order model's correlation coefficient (R^2) values were nearer to unity (for AY 49 = 0.999 and RO 12 = 0.999), suggesting that the model is better suited to explain the way AY 49 and RO 12 dye adsorb onto Amberlite IRA-400(Cl^-) resin. The experimental adsorption capacity (qe, exp) for the pseudo-second-order model matched the calculated adsorption capacity (qe, cal) presented in **Table 4.2**. Literature [49] confirmed the applicability of the pseudo-second-order kinetic model for sorption of AY 49 and RO 12 dyes on Amberlite IRA-400(Cl^-) resin.

The intraparticle diffusion model controls the sorption when the graph of q_t against $t^{0.5}$ is a straight line passing through the origin [50]. The R^2 values were less than that derived from the pseudo-second order kinetic model presented in **Table 4.2**. The plot of q_t vs $t^{1/2}$ in **Figure 4.15 (c) and 4.16 (c)** exhibits an empirical relationship indicating the sorbate uptake in relation to the square root of time. The Weber-Morris plot, yet, indicates that the fitting of experimental data should follow linearity; however, in this particular example, deviation from a linear plot is anticipated because of the resistance supplied by the boundary layer.

Table 4.2. Kinetic parameters of dye adsorption onto Amberlite IRA-400(Cl^-) resin.

Models	Parameters	AY 49	RO 12
Pseudo-first-order	k_1	-0.0014	-0.0005
	q_e (cal)	1.900	1.166
	R^2	0.716	0.792
Pseudo-second-order	k_2	0.038	0.029
	q_e (cal)	15.57	15.29
	R^2	0.999	0.999
Interparticle diffusion	k_{id}	0.305	0.358
	c	11.90	10.95
	R^2	0.501	0.511
Experimental	q_e (exp)	15.28	15.15

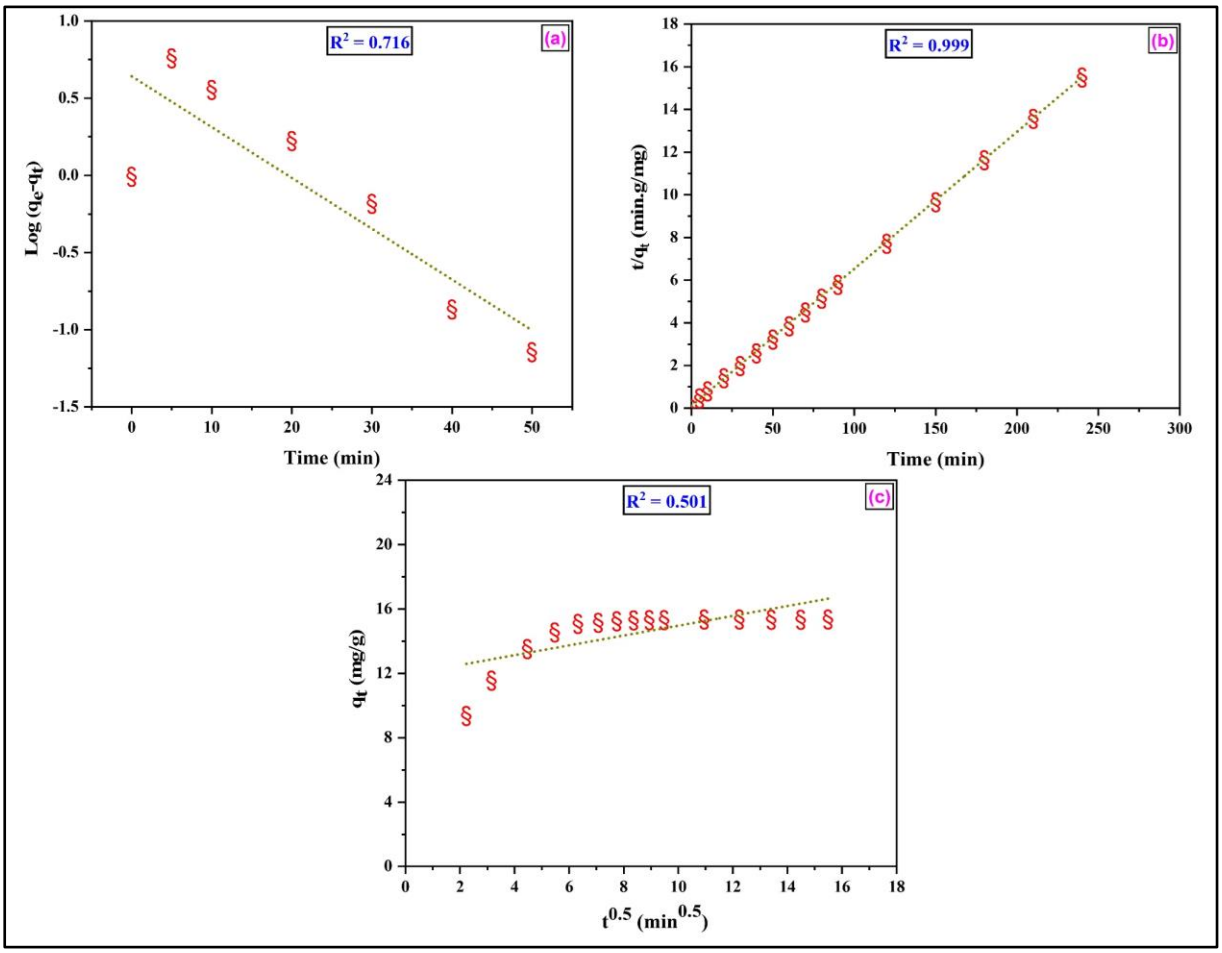

Figure 4.15. Pseudo-first-order (a), pseudo-second-order (b), and intraparticle diffusion (c) model using the AY 49@Amberlite IRA-400(Cl^-) resin.

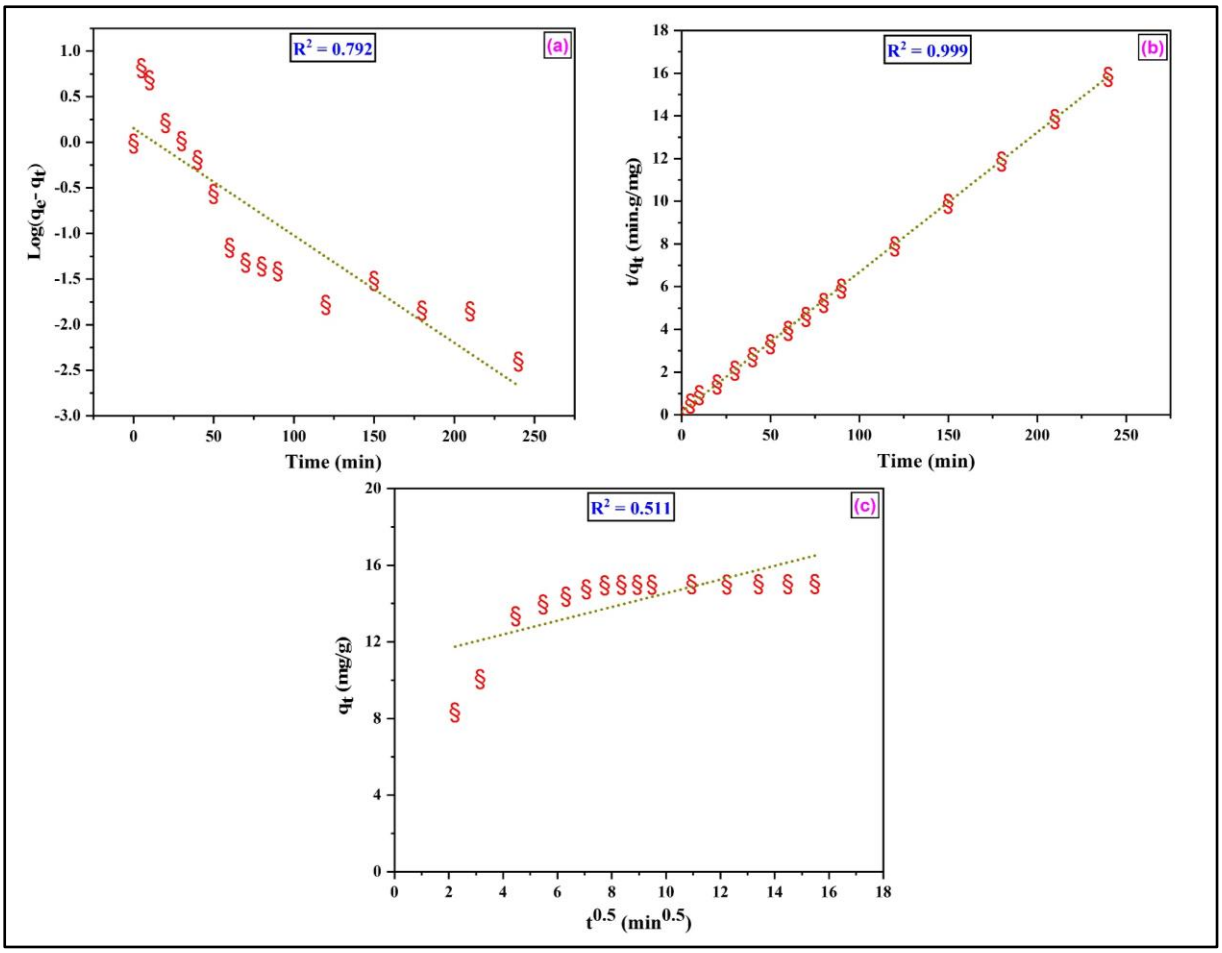

Figure 4.16. Pseudo-first-order (a), pseudo-second-order (b), and intraparticle diffusion (c) model using the RO 12@Amberlite IRA-400(Cl^-) resin.

4.3.2.8. Thermodynamics study

The adsorption of AY 49 and RO 12 by the Amberlite IRA 400(Cl^-) resin can be better understood by examining thermodynamic parameters. The nature of the current study is shown by the assessment and examine of thermodynamic variables such as free energy change (ΔG^o), enthalpy and entropy change (ΔH^o, ΔS^o), which are depicted in **Figure 4.17** and whose values are presented in **Table 4.3**. It is demonstrated that the adsorption of RO 12 and AY 49 by physical force is feasible and spontaneous by the negative value of ΔG^o and its decrease with rising temperatures. The positive value of ΔH^o shows that the procedure is endothermic and the positive value of ΔS^o indicated a greater stability of adsorption process at the solid–liquid interface, confirming the spontaneity of the process [51].

Table 4.3. Thermodynamic parameters evaluated at different temperatures using Amberlite IRA-400 (Cl^-) resin.

Dyes	Temperature (K)	ΔG^o (kJ.mol^{-1})	ΔH^o (kJ.mol^{-1})	ΔS^o (J.mol^{-1}.$^oC^{-1}$)
AY 49	303	-5.186	26.35	106.17
	313	-7.765		
	323	-8.203		
	333	-8.481		
RO 12	303	-5.551	7.04	41.92
	313	-6.240		
	323	-6.524		
	333	-6.838		

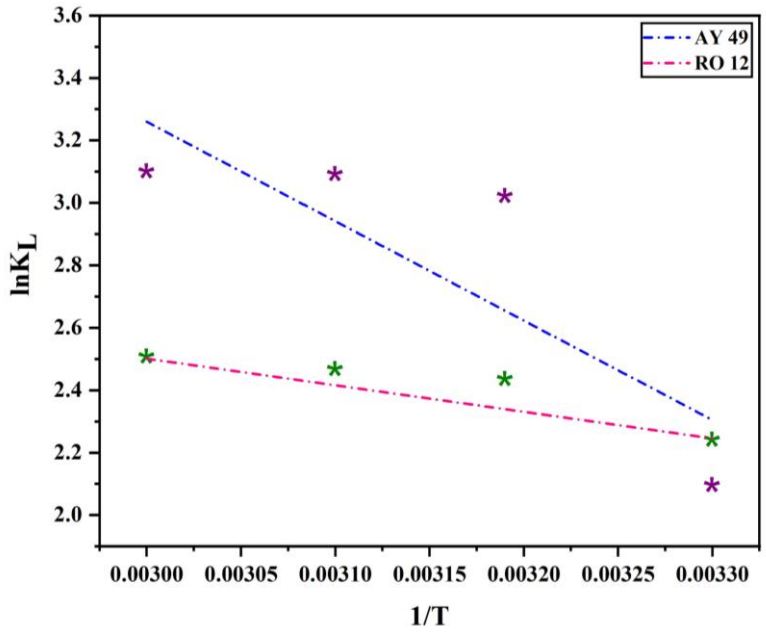

Figure 4.15. Thermodynamic of evaluated at different temperatures using AY 49@ Amberlite IRA-400(Cl^-) resin and RO 12@Amberlite IRA-400(Cl^-) resin.

4.4. Conclusions

The present work studied the adsorbent properties of Amberlite IRA-400(Cl^-) resin on AY 49 and RO 12 removal. It's characterized by using SEM, FTIR, UV, EDX. Through batch studies, after AY 49 and RO 12 sorption on adsorbent were optimized to be natural pH (AY 49 (4.15) and RO 12 (4.07)), dose of adsorbent (80 mg), initial concentration (50 mg/L), and duration of time (40 min). Isotherm modelling, based on R^2 values, showed that the Freundlich model, in comparison to other models, could more accurately predict the adsorption of dye onto the Amberlite IRA-400(Cl^-) resin.

The monolayer sorption capabilities of Amberlite IRA-400(Cl^-) resin towards Acid Yellow 49 (2000 mg/g) and Reactive Orange 12 (175.43 mg/g) indicate that this resin may be a suitable adsorbent for the treatment of textile wastewater. The following is an outline of the dye affinity series for quaternary ammonium functionality in Amberlite IRA-400(Cl^-) resin:

Acid Yellow 49 (AY 49) > Reactive Orange 12 (RO 12)

Kinetics studies reveal that the adsorption shows the best with pseudo-second-order model. Investigations of thermodynamics demonstrated that the adsorption process was spontaneous and endothermic. It was demonstrated that Amberlite IRA-400(Cl^-) resin can efficiently remove AY 49 and RO 12 dye. This resin seems to serve as a suitable adsorbent for the treatment of textile effluent to remove dyes.

4.5. References

[1] S.M. Siddeeg, M.A. Tahoon, N.S. Alsaiari, M. Shabbir, F.B. Rebah, Current Analy. Chemist. **17** (2021) 4–22.

[2] M. Wawrzkiewicz, Ind. Eng. Chem. Res. **51** (2012) 8069−8078.

[3] A. Kumar, M. Sehgal, SAE International: Warrendale, PA, USA, 2018.

[4] J. Aguilar-Rosero, M.E. Urbina-Lopez, B.E. Rodrıguez-Gonz´alez, S.X. Le´on-Villegas, I.E. Luna-Cruz, and D.L. Cardenas-Ch´avez, App. Sci. **12(5)** (2022) 2740.

[5] F. Marrakchi, B.H. Hameed, E.H. Hummadi, Int. J. Biol. Macromol. **163** (2020) 1079–1086.

[6] M.M. Hassan, C.M. Carr, Chemosphere **209** (2018) 211–219.

[7] S. Ghuge, A. Saroha, Int. J. Environ. Waste Manag. **1** (2022) 1–8.

[8] M. Deaconu, R. Senin, Int. J. Waste Resour. 2016, 6.

[9] K. M. Katubi, F. M. Alzahrani, N. S. Alsaiari, A. Amari, F. B. Rebah, and M. A. Tahoon, Processes, **9(5)** (2021) 818.

[10] Y. Zhou, J. Lu, Y. Zhou, Y. Liu, Environ. Pollut. **252** (2019) 352–365.

[11] V. Gomez, M.S. Larrechi, M.P. Callao, Chemosphere **69(7)** (2007) 1151–1158.

[12] H.Z. Chen, Ind. Eng. Chem. Res. **51(43)** (2012) 14026–14036.

[13] R. Mogale, K.G. Akpomie, J. Conradie, E.H.G. Langner, J. Environ. Manag. **304** (2022) 114166.

[14] Y. Hu, T. Guo, X. Ye, Q. Li, M. Guo, H. Liu, Z. Wu, Chem. Eng. J. **228** (2013) 392–397.

[15] K. Dorfner, Ion Exchange. Walter de Gruyter, Berlin, New York, 1991.

[16] S. Karcher, R.A. Kornmülle, M. Jekel, Dyes Pigments **51** (2001) 111–125.

[17] T.L. Silva, A.L. Cazetta, P.S.C. Souza, T. Zhang, T. Asefa, V.C. Almeida, J. Clean. Prod. **171** (2018) 482–490.

[18] W. Song, B. Gao, X. Xu, L. Xing, S. Han, P. Duan, R. Jia, Bioresour. Technol. **210** (2016) 123-130.

[19] S. Karcher, A. Kornmüller, M. Jekel, Water Res. **36** (2002) 4717–4724.

[20] M. Wawrzkiewicz, Z. Hubicki, Solvent Ext. Ion Exch. **34** (2016) 558–575.

[21] M. Greluk, Z. Hubicki, Chem. Eng. J. **215–216** (2013) 731–739.

[22] E. Polska-Adach, M. Wawrzkiewicz, Z. Hubicki, Physicochem. Probl. Miner. Process. **55** (2019) 1496–1508.

[23] M. Wawrzkiewicz, Z. Hubicki, Chem. Eng. J. **157** (2010) 29–34.

[24] M. Wawrzkiewicz, Z. Hubicki, Open Chem. **9** (2011) 867–876.

[25] K. Wrzesi´nska, M. Wawrzkiewicz, K. Szymczyk, J. Mol. Liq. **331** (2021) 115748.

[26] I. Langmuir, J. of Ame. Chem. Soc. **38(11)** (1916), 2221–2295.

[27] A.F. Dashti, H.A. Aziz, M.N. Adlan, A.H. Ibrahim, Int. J. Environ. Sci. Technol. **16** (2019) 6419–6430.

[28] I.A.W.A.W. Tan, A.L.L. Ahmad, B.H.H. Hameed, J. Hazard. Mater. **154** (2008) 337–346.

[29] H. M. Over the adsorption in solution. J. Phys. Chem. **57** (1906) 385–470.

[30] R. Das, A. Mukherjee, I. Sinha, K. Roy, B.K. Dutta, Appl. Water Sci. **10** (2020) 117.

[31] F. Batool, J. Akbar, S. Iqbal, S. Noreen, S. Nasir, A. Bukhari, Bioinorg. Chem. Appl. **3** (2018) 230–239.

[32] L. Toledo, B.L. Rivas, B.F. Urbano, J. Sánchez, Sep. Purif. Technol. **103** (2013) 1-7.

[33] M. Wawrzkiewicz, Z. Hubicki, J. of Hazard. Mater. **172** (2009) 868–874.

[34] C. Clavijo, J.F. Osma, Water **11** (2019) 1906.

[35] P.D. Egwuonwu, Acad. Res. Int. **4** (2013) 330.

[36] V. Dulman, C. Simion, A. Bârsănescu, I. Bunia, V. Neagu. J. Appl. Poly. Sci. **113** (2009) 615–627.

[37] M. Ghaedi, F. Karimi, B. Barazesh, R. Sahraei, A. Daneshfar. J. of Ind. and Engg. Chem. **19** (2013) 756–763.

[38] D. Vara, S. Jha, S. Bisht, S. Shahabuddin, R. Gaur, S.I. Tyagi. Toxics **12** (2024) 266.

[39] Z. Eren, F.N. Acar, Desalination **194** (1–3) (2006) 1–10.

[40] M.A. Ashraf, M. Hussain, K. Mahmood, A. Wajid, M. Yusof, Y. Alias, I. Yusoff. Desalin. Water Treat. **51** (2013) 4530–4545.

[41] M. Wawrzkiewicz, Ind. & Engg. Chem. Res. **53** (2014) 11838.

[42] N. M. Marin, L. F. Pascu, A. Demba, M. Nita-Lazar, I. A. Badea, H. Y. Aboul-Enein. Int. J. of Environ. Sci. and Technol. **16** (2019) 6357–6366

[43] M. Wawrzkiewicz, Z. Hubicki, Environ. Technol. **30** (2009) 1059–1071.

[44] H. Lata, V.K. Garg, R.K. Gupta, Desalination **219** (2008) 250–261.

[45] M. Wawrzkiewicz, E. Polska-Adach, Water **13** (2021) 385.

[46] M. Greluk, Z. Hubicki, Desalination **278** (2011) 219–226.

[47] M. Wawrzkiewicz, Z. Hubicki, J. Hazard. Mater. **164** (2009) 502–509.

[48] Z. Zhu, M. Zhang, F. Liu, C. Shuang, C. Zhu, Y. Zhang, A. Li, J. Taiwan Inst. Chem. Eng. **62** (2016) 98–103.

[49] S. Sinha, S.S. Behera, S. Das, A. Basu, R.K. Mohapatra, B.M. Murmu, N.K. Dhal, S. K. Tripathy, P.K. Parhi, Chem. Engg. Comm. **205(4)** (2018) 432-444.

[50] S.S. Gupta, K.G. Bhattacharyya, Adv. Colloid. Interface Sci. **162** (2011) 39–58.

[51] A.A. Inyinbor and F.A.A.G.A. Olatunji, Appl. Water Sci. **7** (2017) 2297–2307.